CrossMark

Cold Giant Planets Evaporated by Hot White Dwarfs

Matthias R. Schreiber[1,2] , Boris T. Gänsicke[3,4], Odette Toloza[3], Mercedes-S. Hernandez[1], and Felipe Lagos[1,2]
[1] Instituto de Física y Astronomía, Universidad de Valparaíso, Valparaíso, Chile; matthias.schreiber@uv.cl
[2] Millennium Nucleus for Planet Formation, NPF, Universidad de Valparaíso, Valparaíso, Chile
[3] Department of Physics, University of Warwick, Coventry CV4 7AL, UK
[4] Centre for Exoplanets and Habitability, University of Warwick, Coventry CV4 7AL, UK

Abstract

Atmospheric escape from close-in Neptunes and hot Jupiters around Sun-like stars driven by extreme ultraviolet (EUV) irradiation plays an important role in the evolution of exoplanets and in shaping their ensemble properties. Intermediate and low mass stars are brightest at EUV wavelengths at the very end of their lives, after they have expelled their envelopes and evolved into hot white dwarfs. Yet the effect of the intense EUV irradiation of giant planets orbiting young white dwarfs has not been assessed. We show that the giant planets in the solar system will experience significant hydrodynamic escape caused by the EUV irradiation from the white dwarf left behind by the Sun. A fraction of the evaporated volatiles will be accreted by the solar white dwarf, resulting in detectable photospheric absorption lines. As a large number of the currently known extrasolar giant planets will survive the metamorphosis of their host stars into white dwarfs, observational signatures of accretion from evaporating planetary atmospheres are expected to be common. In fact, one-third of the known hot single white dwarfs show photospheric absorption lines of volatile elements, which we argue are indicative of ongoing accretion from evaporating planets. The fraction of volatile contaminated hot white dwarfs strongly decreases as they cool. We show that accretion from evaporating planetary atmospheres naturally explains this temperature dependence if more than 50% of hot white dwarfs still host giant planets.

1. Introduction

Atmospheric escape has been a key topic in exoplanet research since Mayor & Queloz (1995) speculated that the hot Jupiter 51 Peg b might be a radiatively stripped brown dwarf. Direct evidence for the escape of atmospheric hydrogen was first established by *Hubble Space Telescope* Lyα transit spectroscopy of the hot Jupiter HD 209458 (Vidal-Madjar et al. 2003), later for close-in Neptunes (Ehrenreich et al. 2015; Bourrier et al. 2018), and possibly super-Earths (Ehrenreich et al. 2012). Outflowing atmospheres have also been detected from large transit depths in the far-ultraviolet resonance lines of O I and C II (Vidal-Madjar et al. 2004; Ben-Jaffel & Ballester 2013).

This atmospheric escape is driven by high-energy irradiation. Extreme ultraviolet (EUV, $\lambda = 100$–912 Å) photons have sufficient energy to directly ionize hydrogen atoms ($h\nu = 13.6$ eV). A significant fraction of the energy of the generated photoelectrons is converted into heat as radiative cooling is inefficient. This drives the atmosphere out of hydrostatic equilibrium into a transonic flow (Parker 1964; Tian et al. 2005). If the resulting escape flow of hydrogen is large enough, drag forces carry along heavier constituents of the atmosphere, as indicated by the observations (Yelle et al. 2008; Vidal-Madjar et al. 2004; Ben-Jaffel & Ballester 2013).

As the mass loss rate increases with the amount of incident ionizing EUV radiation, hydrodynamic escape is expected to be important especially for planets around stars younger than $\simeq 100$ million years, which have EUV fluxes 100–1000 times that of the present-day Sun (Ayres 1997; Tu et al. 2015). Planet evaporation during these early phases of large host-star EUV luminosities is thought to explain both the dearth of Neptune mass planets with orbital periods shorter than ∼10 days, referred to as the "warm Neptune desert," as well as the low occurrence of planets with radii of $\simeq 2R_{\mathrm{Earth}}$ at separations of 0.03–0.1 au, usually termed "the evaporation valley" (Owen & Wu 2017).

One phase of stellar evolution where the large EUV luminosity of the host stars can drive significant atmospheric escape from giant planets has been overlooked so far: the very last stages of the evolution of planetary systems when the host star will have evolved into a hot white dwarf. The survival of planetary systems into the white dwarf stage is demonstrated by the detection of the debris from tidally disrupted planetesimals (Jura 2003; Zuckerman et al. 2003; Koester et al. 2014). Here we show that the EUV emission from hot white dwarfs may have far-reaching consequences for the future of the solar system as well as important implications for our understanding of metal pollution in hot white dwarfs.

2. The Future of the Solar System

The Sun will slowly lose about half of its mass during the evolution through the giant branches, causing the giant planets to spiral out—while remaining gravitationally bound—to roughly twice their current orbital separations (Duncan & Lissauer 1998). The solar white dwarf will initially have an effective temperature of $\gtrsim 100{,}000$ K and cool quasi-exponentially to $\simeq 55{,}000$ K within 1 Myr, and to $\simeq 30{,}000$ K within 10 Myr (Fontaine et al. 2001). Consequently, the solar white dwarf remains a luminous EUV source for several million years.

2.1. The EUV Luminosity of the Solar White Dwarf

To establish the EUV luminosity of the solar white dwarf, we computed a grid of synthetic spectra extending from 10 to 25,000 Å using the model atmosphere code of Koester (2010). The atmospheric input parameters are the effective temperature
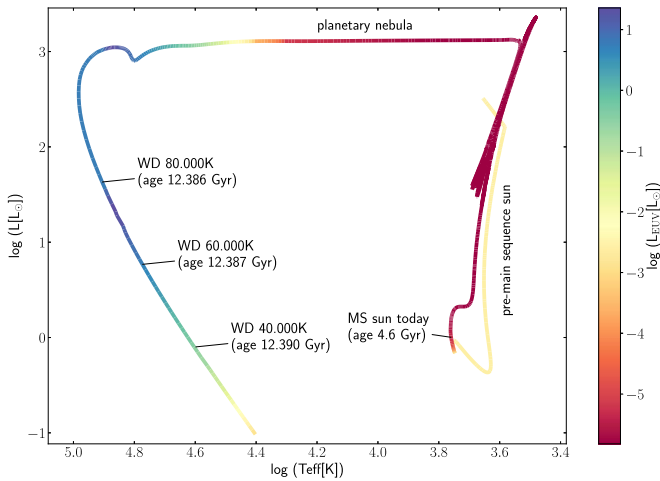
Figure 1. Evolution of the EUV luminosity of the Sun across the Hertzsprung–Russel diagram. During the pre-main-sequence phase, the EUV luminosity reaches $\simeq 0.1\%$–0.5% of the solar luminosity, and drops significantly during the main sequence and the giant branches. However, once the star expelled its envelope during the planetary nebular phase, its hot degenerate core—the white dwarf—is exposed, which for a few million years emits almost all its radiation in the EUV, resulting in $L_{\rm EUV} \gg L_\odot$.

($T_{\rm eff}$) and surface gravity ($\log g$) of the white dwarf. For a fixed mass, the white dwarf slightly contracts as it cools, and hence its surface gravity increases with time. We therefore interpolated the cooling tracks of Holberg & Bergeron (2006) for $M_{\rm wd} = 0.5\,M_\odot$ to determine $T_{\rm eff}$, $\log g$, the white dwarf radius and its cooling age.

We computed the synthetic spectra assuming pure hydrogen atmospheres. The presence of metals in the atmosphere will modify the emerging spectral energy distribution, in particular iron, which has a large number of absorption lines in the EUV. This additional opacity is blocking the outgoing flux at short wavelengths, redistributing the energy to longer wavelengths. However, even with trace metals in their atmospheres, hot white dwarfs remain luminous EUV sources (see Figure 5 of Chayer et al. 1995).

The evolution of the EUV luminosity of the Sun from the pre-main sequence into the white dwarf cooling track[5] is illustrated in Figure 1. We assumed $L_{\rm EUV} = 10^{31}$ erg s^{-1} for the pre-main-sequence phase, which most likely represents an upper limit (Tu et al. 2015). For the EUV luminosity on the main sequence we used Equation (4) of Sanz-Forcada et al. (2011) and extended this relation to the giant-branch, which should result in approximately correct EUV luminosities (Pizzolato et al. 2000). For simplicity we interpolated the EUV flux from the planetary nebula phase to our first white dwarf model. The EUV flux for the white dwarf phase was determined integrating the synthetic spectra from 100 to 912 Å. For the initial few million years, the EUV luminosity of the solar white dwarf will exceed that of the present-day Sun by 10^5–10^6, and that of the young, chromospherically active Sun by 10^2–10^3. The extreme EUV luminosity of the solar white dwarf will drive atmospheric mass loss from the giant planets that survived the metamorphosis of the Sun.

2.2. Photoevaporation of the Giant Planets

Motivated by the detections of extended atmospheres of hot Jupiters and close-in Neptunes, hydrodynamic calculations of

---

[5] The stellar evolution track was calculated with MESA (Paxton et al. 2011).

EUV irradiated hydrogen atmospheres have been developed throughout the last decade (Yelle et al. 2008; Murray-Clay et al. 2009; Owen & Alvarez 2016). According to these models, the hydrodynamic wind generated by EUV radiation can be separated into two different regimes. At lower fluxes, lower densities result in relatively long recombination times, adiabatic expansion dominates the gas cooling, and the wind mass loss rate is proportional to the incident EUV flux. This regime is called *energy limited*. At high fluxes, the recombination timescale decreases and the wind mass loss scales approximately with the square root of the incident EUV flux (see Owen 2019, for details). This regime is called *recombination limited*. Many variants of equations describing energy limited hydrodynamic escape appear in the literature, and we use the expression

$$\dot{M}_{\rm elim} = \frac{\beta \pi F_{\rm EUV} R_{\rm P}^3}{G M_{\rm P}}, \qquad (1)$$

where $M_{\rm P}$ and $R_{\rm P}$ are the mass and radius of the planet, $F_{\rm EUV}$ is the incident EUV flux, G is the gravitational constant, and β is an efficiency parameter which is typically adopted to be $\simeq 0.2$ (Murray-Clay et al. 2009).

The transition from the recombination limited regime into the energy limited regime occurs over a range of limiting fluxes and depends on the mass and radius of the planet (Owen & Alvarez 2016). For simplicity, we assume a flux of $F_{\rm EUV} = 10^4$ erg s^{-1} for this transition, as suggested for the case of a hot Jupiter by Murray-Clay et al. (2009). To ensure the robustness of our results, we repeated our analysis with several different prescriptions, e.g., a flux limit of $F_{\rm EUV} = 10^3$ erg s^{-1} for cold Jupiters, a much higher limit of $F_{\rm EUV} = 10^5$ erg s^{-1} for Neptune mass planets (Owen & Alvarez 2016), and a linear interpolation in between. Our results are not affected by the choice of the flux at which the transition occurs.

Figure 2 compares the incident EUV flux from the current Sun, the young and active Sun, and the solar white dwarf for temperatures in the range of 80,000–30,000 K, as a function of the semimajor axis. The very large EUV irradiation from the white dwarf will drive mass loss rates of $\dot{M} \sim 10^8$–10^{11} g s^{-1} from all giant planets in the solar system, despite their large orbital separations. These mass loss rates are comparable to those measured for hot Jupiters and warm Neptunes (e.g., Vidal-Madjar et al. 2003; Ehrenreich et al. 2015). While surprising at first, this result is a simple consequence of the large EUV luminosity of the white dwarf, 10^5–10^6 that of the present-day Sun, which compensates for the 10^2–10^3 times larger separation of the surviving planets compared to the short-period evaporating planets found around main-sequence stars.

2.3. Observational Signatures of Giant Planet Evaporation

Given their large surface gravity, white dwarfs rapidly undergo chemical stratification via gravitational settling (Schatzman 1948), and their atmospheres are expected to be composed of the lightest elements, hydrogen or helium. Nevertheless, photospheric trace metals are commonly observed in the ultraviolet and optical spectra of cool ($T_{\rm eff} \lesssim 20{,}000$ K) white dwarfs (Zuckerman et al. 2003; Jura & Young 2014; Koester et al. 2014), and it is now well-established that these white dwarfs accrete the debris of tidally disrupted planetesimals (Jura 2003; Farihi 2016; Veras 2016).
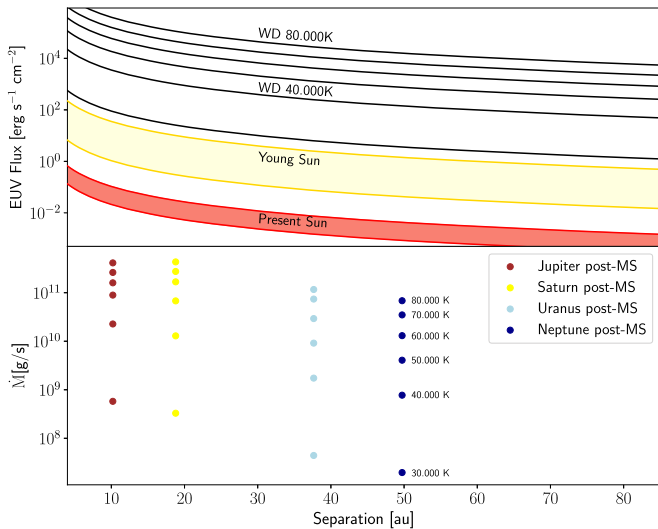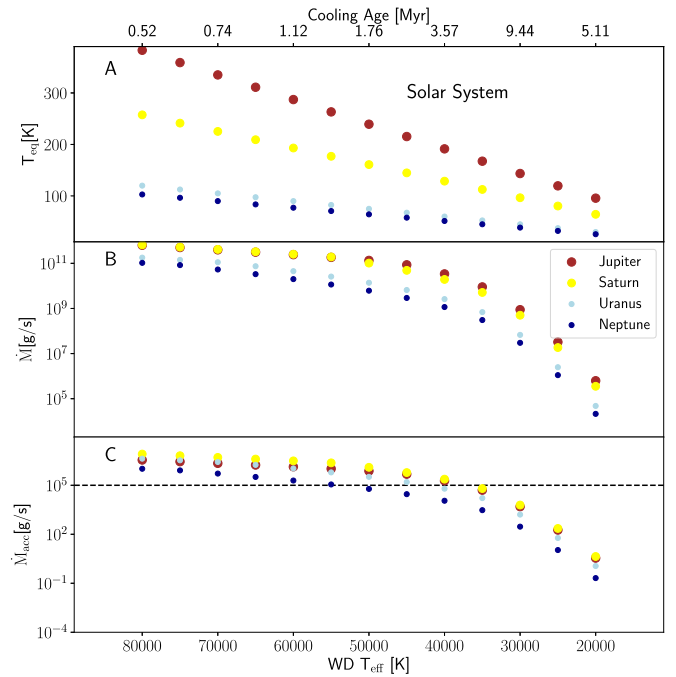
Figure 2. Top panel: comparison of the incident EUV flux per unit area onto giant planets as a function of the orbital separation. The irradiating flux from hot white dwarfs (80,000–30,000 K) can exceed those of the young Sun by many orders of magnitude. This intense EUV radiation can cause atmospheric escape in giant planets located at separations as large as ≃100 au. Bottom panel: estimated mass loss of the giant planets in our solar system once the Sun has transformed into a white dwarf for temperatures of 80,000–30,000 K. The mass loss rates of the giant planets orbiting the young solar white dwarf are comparable to those observed from exoplanets on close-in orbits around main-sequence stars.

Figure 3. Top panel: the equilibrium temperatures, mass loss rates, and accretion rates onto the solar white dwarf for the four giant planets as a function of its effective temperature. The corresponding cooling ages are given on the top axis. Given their large separations from their host white dwarf, the equilibrium temperatures of the planets are relatively low and monotonously decrease as the white dwarf cools. Middle panel: the mass loss rates driven by the EUV irradiation will remain high, 10^{11}–10^9 g s^{-1}, for white dwarf temperatures exceeding ≃45,000 K and drop by 2–4 orders of magnitude for cooler white dwarfs. Bottom panel: the accretion rate of metals will detectable for $\dot{M}_{\rm acc} \gtrsim 10^5$ g s^{-1} (i.e., for $T_{\rm eff} \gtrsim 45,000$ K, dashed line) for ≃4 Myr after the formation of the white dwarf.

The solar white dwarf will capture a fraction of the material escaping the atmospheres of the giant planets that survived the Sun's post-main-sequence evolution. Taking into account that the flow is supersonic, the Hoyle–Littleton approach is applicable (Shapiro & Lightman 1976; Wang 1981). The white dwarf will accrete material within a cylinder of radius $r_a = \psi 2GM/v_{\rm rel}$ with ψ being a factor of order unity representing deviations from the Hoyle–Littleton prescription, and $v_{\rm rel}$ being the relative velocity between the white dwarf and the wind. The resulting accretion rate can then be written as (Shapiro & Lightman 1976; Wang 1981):

$$\dot{M}_{\rm acc} \simeq \pi \, r_a^2 \, \rho(a) v_{\rm rel}(a), \qquad (2)$$

where a is the separation of the planet, and the relative velocity can be approximated as $v_{\rm rel}(a) = (v_{\rm evap}^2 + v_{\rm x}^2)^{1/2}$ with $v_{\rm evap}$ being the wind velocity and $v_{\rm x} = 2 \pi a/P_{\rm orb}$. The density of the outflow can be estimated assuming spherically symmetric mass loss of the planet, $\rho = \dot{M}_{\rm evap}/(4\pi a^2)$. For a given mass loss rate from the planet, the resulting mass accretion rate onto the white dwarf depends critically on $v_{\rm rel}$, thus on the wind velocity $v_{\rm evap}$, which we assumed to be constant. This quantity is largely unknown. Detailed models of hydrodynamic escape show that the escape velocity is typically reached at separations of a few times the radius of the planet (Tian et al. 2005; Tripathi et al. 2015). We here assume the wind velocity to be equal to the escape velocity at four times the planets radius and note that our main conclusions are not very sensitive to this assumption, i.e., varying the velocity by a factor of two does not lead to significant changes.

While the ionization of hydrogen drives the hydrodynamic escape, only the heavier elements dragged with the flow will be accreted by the white dwarf: Lyα radiation pressure from hot white dwarfs substantially exceeds the gravitational attraction,

and effectively prevents the inflow of hydrogen onto the white dwarf (Brown et al. 2017). As little is known regarding the exact composition of the evaporated material, we adopted solar metallicity, i.e., a metal mass fraction of 2%, for the calculation of the accretion rate of metals onto the white dwarf.

We find initial metal accretion rates onto the white dwarf of ≃10^8 g s^{-1} and a gradual decrease for 4 Myr to ≃10^5 g s^{-1} as the white dwarf cools to ≃45,000 K (Figure 3). For cooler white dwarfs, the peak of their spectral energy distribution shifts from the EUV into the ultraviolet, and hence both its efficiency at evaporating the giant planet atmospheres, and the resulting accretion rate onto the white dwarf drops more steeply.

Given that white dwarf atmospheres are intrinsically devoid of metals, optical and ultraviolet spectroscopy is sensitive to the detection of traces of accreted planetary material, corresponding to accretion rates of as little as 10^5 g s^{-1} (Koester et al. 2014). We conclude that the solar white dwarf will accrete significant amounts of volatiles from the evaporating giant planets and the accreted planetary material will be spectroscopically detectable by future generations of alien astronomers for several million years.

3. Photospheric Volatiles at Hot White Dwarfs

The detection of photospheric metals in hot ($\gtrsim$20,000 K) white dwarfs is challenging from the ground, as few elements have sufficiently strong optical transitions. However, ultraviolet spectroscopy obtained with the *International Ultraviolet Explorer*

revealed strong photospheric metal lines in several hot white dwarfs (Bruhweiler & Kondo 1981). Subsequent studies with the *Hubble Space Telescope* and the *Far Ultraviolet Spectroscopic Explorer* showed photospheric trace metals in many white dwarfs hotter than $\simeq 50,000$ K (e.g., Barstow et al. 2003).

In contrast to cool white dwarfs, where the photospheric abundances reflect the rocky nature of the accreted material (Xu et al. 2014), these hot white dwarfs show large abundances of volatiles, in particular C, S, and P. Whereas the interpretation of these observations is more complex than for cooler white dwarfs because of radiative forces counteracting gravitational settling, the consensus is that the abundances determined from the observations do not match the predictions of equilibrium radiative levitation theory (Chayer et al. 1995). In the most comprehensive far-ultraviolet study of hot white dwarfs, Barstow et al. (2014) detected photospheric C, P, or S in 33 out of 89 white dwarfs. Barstow et al. (2014) reiterated that the observed pattern of abundances is incompatible with the predictions of radiative levitation, and concluded that accretion of planetary debris is the most likely explanation. The presence of reservoirs of this material is corroborated by the detection of circumstellar absorption lines (Dickinson et al. 2013), which are only present in the spectra of hot white dwarfs that also show photospheric trace metals.

We argue that the volatiles detected among about a third of the hot ($T_{\rm eff} \gtrsim 20,000$ K) white dwarfs with adequate ultraviolet spectroscopy, and their observed increasing abundances with $T_{\rm eff}$, are the signature of evaporating giant planets (gas or ice giants planets from super-Earths to Jupiters). This hypothesis implies that a significant fraction of white dwarf progenitor stars hosted giant planets at separations large enough to survive their post-main-sequence evolution.

4. Planet Occurrences at Large Separations around A&F Stars

Most of the currently known white dwarfs had progenitors with masses of 1.5–2.5 $M_\odot$ and spectral types F to A. Direct imaging revealed the existence of Jupiter mass giant planets at larger separations (5–100 au) around young A-type stars (e.g., Marois et al. 2008; Chauvin et al. 2017). Recent radial velocity studies indicate an increase in both the occurrence rate and orbital separations of Jupiter mass planets with increasing stellar mass (Borgniet et al. 2019). Surveys targeting subgiant stars with $M \geqslant 1.6 M_\odot$, the so-called "retired A stars," confirm this trend: the giant planet occurrence increases with stellar mass up to $\simeq 2 M_\odot$ (Ghezzi et al. 2018). Just as in the solar system, these giants planets will survive the evolution of their host stars into white dwarfs.

Currently the only method capable of detecting Neptune mass planets at large orbital separations from their host star is microlensing. Whereas microlensing surveys confirm the relatively low occurrence rates for Jupiter mass planets they consistently find large occurrence rates for Neptune and super-Earth mass planets. The fraction of bound planets at distances of 0.5–10 au from their host stars was found to be $17^{+6}_{-9}\%$ in the mass range 0.3–10 $M_{\rm Jup}$ but significantly larger, $52^{+22}_{-29}\%$ and $62^{+35}_{-37}\%$, for Neptunes and super-Earths, respectively (Cassan et al. 2012). While this study relied on a small sample of events (Suzuki et al. 2016), the main conclusions have been independently confirmed (e.g., Shvartzvald et al. 2016).
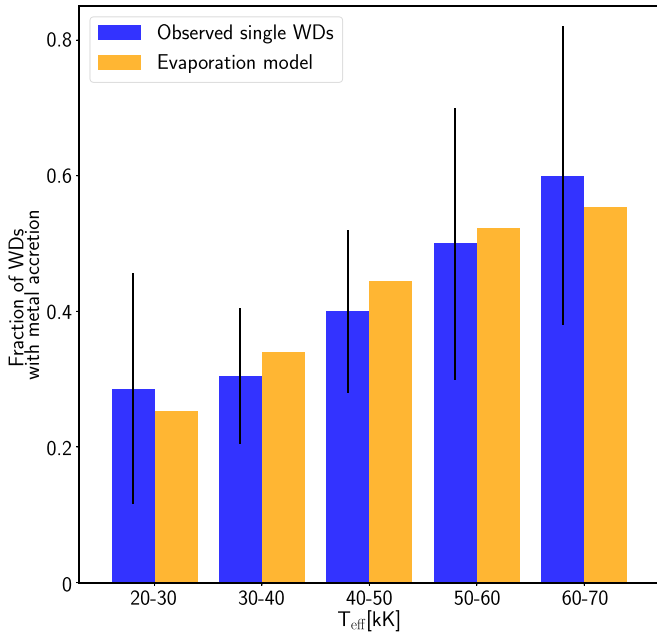
5. A Planet Population Model

Based on the observational evidence for a rising occurrence rate of Jupiter mass planets with increasing stellar mass, we extrapolated from the microlensing surveys that mostly target K- and M-dwarfs to the fraction of A- and F-type stars with Neptune mass planets beyond the snow-line to test our hypothesis that many hot white dwarfs are evaporating giant planets, and accrete some of their atmospheric material.

For this test we use only the single stars of Barstow et al. (2014), as binarity affects the statistics for two reasons. On one hand, stellar winds from relatively close main-sequence companions can cause metal pollution (Pyrzas et al. 2012) which is then impossible to distinguish from accretion of evaporated planetary atmospheres. On the other hand, the formation of giant planets can be impeded by the presence of close and/or massive stellar companions. Holberg et al. (2013) list stellar companions for 20 of the 89 systems of Barstow et al. (2014); however, this compilation ignored M-type companions. Scrutiny of the literature reveals one additional wide binary (WD 0501+524) and three short-period white dwarf plus M-dwarf binaries. We also identified five new common proper motion companions using a 2 arcmin search within the *Gaia* Data Release 2 (*Gaia* Collaboration et al. 2018). Finally, we removed WD 0802+413 and WD 0621 −376 from the sample. While there is no clear evidence that they are part of binaries, their masses are too low to have evolved as single stars within the age of the Galaxy.

Using the final sample of 58 white dwarfs, we then performed Monte-Carlo simulations to test the suggested scenario. We constructed a planet population model for the white dwarf progenitor stars with initial semimajor axes of 3–30 au. For the probability distributions of planet mass ratio and separation we used the equations and best-fit values from recent microlensing planet surveys (Suzuki et al. 2016, their Table 4).

The planet positions after the evolution of the host star into a white dwarf were determined assuming adiabatic mass loss. We computed the EUV luminosity of each white dwarf as outlined in Section 2.1. We then calculated for each white dwarf the mass accretion rate of evaporated material and evaluated whether it exceeds the detection limit of 10^5 g s^{-1}. We furthermore randomly selected 25% of the white dwarfs as being in addition metal polluted by rocky planetary debris as indicated by the observations of cool white dwarfs (Koester et al. 2014). The only parameter we adjusted was the occurrence rate of planets with hydrogen-rich atmospheres. We find that the fraction of white dwarfs accreting detectable amounts of volatiles from planetary atmospheres evolves with cooling age, and hence effective temperature, consistent with the observations if at least $\simeq 50\%$ of the hot white dwarfs in the sample host at least one giant planet. Figure 4 shows the observed fraction of polluted hot white dwarfs and the predicted fraction of white dwarfs accreting from evaporating giant planets with hydrogen-rich atmospheres as a function of white dwarf temperature for a planet occurrence rate of 65%. The remarkable agreement shows that evaporation of giant planets, unavoidable in the future solar system, offers a consistent explanation for the volatiles frequently detected in hot white dwarfs.

Determining the detailed abundances of the accreted material will require additional work in the treatment of radiative levitation and systematic deep surveys of a well defined sample of hot white dwarfs, but offers the potential to infer the atmospheric composition of extrasolar giant planets.

Figure 4. Comparison between the observed fraction of photospheric trace metals detected in hot white dwarfs (blue, Barstow et al. 2014) with the predictions of our model population of evaporating giant planets (orange, assuming a planet occurrence rate of 65%). In general the agreement is very good for planet occurrence rates exceeding $\simeq 50\%$.

Appendix A
The Hot White Dwarf Sample

A.1. Single White Dwarfs

For the comparison with our planet population model, we restrict the hot white dwarf sample of Barstow et al. (2014) to single stars. We therefore inspected the literature and carried out a search for common proper motion companions using the *Gaia* Data Release 2 (*Gaia* Collaboration et al. 2018), and identified 29 white dwarfs that have a stellar companion. For our planet population mode, we required the progenitor masses of the single white dwarfs (Table 1). Given the uncertainties on the post-main-sequence mass loss, we computed the average progenitor masses of the 58 single white dwarfs using the initial-to-final mass relations of Weidemann (2000), Catalán et al. (2008), Kalirai et al. (2008), Casewell et al. (2009), and Williams et al. (2009).

A.2. White Dwarfs with Stellar Companions

We include below notes on 29 white dwarfs found to have stellar companions, five of which are new discoveries. The properties of these 29 systems are summarized in Table 2.

Table 1
Single White Dwarfs in the Sample of Barstow et al. (2014)

WD	Metals	T_{eff} (K)	$\log g$ (cgs)	M_{wd} ($M_\odot$)	M_{ms} ($M_\odot$)	$\log(t_{\mathrm{cool}})$ (yr)
0001+433	Y	46205	8.85	1.14	6.45	7.29
0004+330	N	47936	7.77	0.58	1.79	6.31
0027−636	N	60595	7.97	0.70	2.83	6.08
0050−332	Y	34684	7.89	0.60	1.97	6.78
0106−358	Y	28580	7.90	0.59	1.85	7.07
0147+674	N	30120	7.70	0.50	1.05	6.97
0235−125	N	32306	8.44	0.91	4.57	7.47
0236+498	N	33822	8.47	0.93	4.75	7.42
0310−688	N	16181	8.06	0.65	2.40	8.23
0320−539	N	32860	7.66	0.50	1.00	6.82
0346−011	N	42373	9.00	1.21	7.02	7.76
0416+402	N	35227	7.75	0.54	1.41	6.72
0455−282	Y	58080	7.90	0.66	2.51	6.11
0549+158	Y	32780	7.83	0.57	1.65	6.85
0603−483	N	33040	7.80	0.56	1.54	6.83
0621−376[a]	Y	62280	7.22	0.46	0.63	5.25
0715−704	N	44300	7.69	0.54	1.41	6.41
0802+413[a]	N	45394	7.39	0.45	0.56	6.10
0809−728	N	30585	7.90	0.60	1.90	6.95
0830−535	N	29330	7.79	0.54	1.38	7.02
0937+505	N	35552	7.76	0.55	1.46	6.71
1017−138[b]	Y	31340	7.79	0.55	1.44	6.91
1041+580	N	29016	7.79	0.54	1.37	7.04
1057+719	N	39555	7.66	0.52	1.19	6.54
1234+481	N	55570	7.57	0.54	1.34	6.11
1254+223	N	39390	7.77	0.56	1.58	6.57
1314+293	N	49435	7.95	0.67	2.55	6.28
1337+701	Y	20435	7.87	0.55	1.52	7.71
1342+442	Y	66750	7.93	0.69	2.78	5.98
1440+753	N	42400	8.54	0.98	5.16	6.88
1611−084	Y	38500	7.85	0.59	1.88	6.63
1615−154	N	38205	7.90	0.62	2.09	6.65
1620+647	N	30184	7.72	0.51	1.12	6.97
1631+781	N	44559	7.79	0.58	1.78	6.42
1636+351	N	36056	7.71	0.53	1.28	6.68
1648+407	N	37850	7.95	0.64	2.31	6.68
1711+668	N	60900	8.39	0.92	4.66	5.97
1725+586	N	54550	8.49	0.97	5.05	6.12
1800+685	N	43701	7.80	0.59	1.80	6.45
1819+580	Y	45330	7.73	0.56	1.58	6.39
1844−223	N	31470	8.17	0.75	3.22	7.15
1845+683	N	36888	8.12	0.73	3.09	6.85
1917+599	Y	33000	7.90	0.60	1.97	6.85
1942+499	Y	33500	7.86	0.59	1.80	6.82
1950−432	Y	41339	7.85	0.60	1.95	6.53
2000−561	Y	44456	7.54	0.49	0.94	6.37
2004−605	N	44200	8.14	0.76	3.29	6.53
2014−575	N	26579	7.78	0.53	1.27	7.19
2020−425	N	28597	8.54	0.97	5.01	7.80
2032+248	N	19150	7.91	0.57	1.68	7.86
2043−635	N	25971	8.36	0.85	4.07	7.74
2111+498	Y	38866	7.84	0.59	1.85	6.61
2116+736	N	54486	7.76	0.60	1.92	6.16
2124−224	Y	48297	7.69	0.55	1.52	6.29
2146−433	Y	67912	7.58	0.57	1.68	5.83
2152−548	N	45800	7.78	0.58	1.77	6.38
2211−495	Y	65600	7.42	0.52	1.21	5.67
2309+105	Y	51300	7.91	0.65	2.42	6.23
2321−549	Y	45860	7.73	0.56	1.59	6.37
2331−475	Y	56682	7.64	0.56	1.58	6.09

Notes.
[a] WD 0802+413 and WD 0621−376 have very low masses, which at face value are incompatible with single-star evolution within the age of the Galaxy. We therefore did not include these two systems in our planet population model.
[b] WD 1017-138 was mistakenly called WD 1019−141 in Barstow et al. (2014).

Table 2
White Dwarfs in the Sample of Barstow et al. (2014) in Stellar Multiples with N Components

WD	N	Alt. Name	a (au)	Metals	$T_{\rm eff}$ (K)	$\log g$ (cgs)	$M_{\rm wd}$ ($M_\odot$)	$M_{\rm ms}$ ($M_\odot$)	$\log(t_{\rm cool})$ (yr)
0041+092	2	BL Psc	<5.9	N	22113	7.71	0.48	0.86	7.49
0131−164	2		18.5	Y	44850	7.96	0.66	2.49	6.45
0226−615	2	HD 15638	<12.4	N	52301	7.76	0.59	1.87	6.20
0229−481	2	[a]	841.5	Y	63400	7.43	0.52	1.17	5.74
0232+035	2	Feige 24	[b]	Y	62947	7.53	0.54	1.42	5.92
0252−055	2	IP Eri	<7.9	Y	30355	7.26	0.36	*	6.51
0353+284	3	V1092 Tau	<107.7	N	32984	7.87	0.59	1.83	6.85
0354−368	2		368.9	N	53000	8.00	0.70	2.82	6.22
0457−103	2	63 Eri	<4.2	N	22261	7.30	0.34	*	7.09
0501+524	2		4170.0	Y	57340	7.48	0.51	1.14	6.00
0512+326	4	14 Aur C	163.8	Y	42849	8.06	0.71	2.91	6.55
0659+130	2		<143.0	N	39960	8.31	0.85	4.05	6.85
0905−724	2	HD 80230	<9.5	N	21551	7.47	0.39	0.01	7.37
1021+266	2	HD 90052	<11.9	Y	35432	7.48	0.44	0.52	6.61
1024+326	2		<460.6	N	41354	7.59	0.50	1.00	6.47
1029+537	2	[a]	3803.8	Y	44980	7.68	0.54	1.40	6.39
1040+492	2	[a]	6942.5	N	47560	7.62	0.53	1.27	6.30
1109−225	2	β Crt	<7.2	N	36885	7.40	0.43	0.34	6.41
1528+487	2	[a]	1741.6	N	46230	7.70	0.55	1.50	6.35
1550+130	2	NN Ser	[b]	N	39910	6.82	0.30	0.00	0.00
1603+432	2	[a]	938.7	N	36257	7.85	0.59	1.84	6.71
1620−391	2		4456.8	N	24760	7.92	0.59	1.85	7.35
1635+529	5	16 Dra	1475	N	20027	8.14	0.71	2.88	7.96
1734+742	2	29 Dra	<116.1	Y	28795	8.00	0.64	2.33	7.06
1921−566	2		28.4	N	52946	8.16	0.78	3.51	6.21
2011+398	2		[b]	Y	47057	7.74	0.57	1.66	6.33
2124+191	2	IK Peg	[b]	N	33290	8.9	1.16	6.60	7.97
2257−073	3	HD 217411B	<1.7	N	38010	7.84	0.59	1.83	6.64
2350−706	2	HD 223816	87.2	Y	76690	7.83	0.68	2.62	5.78

Notes.
[a] New discoveries.
[b] Short-period post-common envelope binaries.

WD 0041+092 (BL Psc) is a K2V+DA binary that was not resolved in *HST* imaging (Barstow et al. 2001).

WD 0131−164 is a M3.5V+DA binary, resolved in *HST* imaging (Farihi et al. 2006, 2010).

WD 0226−615 is an F6V+DA binary, unresolved in *HST* imaging (Barstow et al. 2001).

WD 0229−481 has a newly identified common proper motion companion, *Gaia* DR2 4939012317940174592. The absolute magnitude of the companion, $G \simeq 10.5$, suggests that it is a late M-dwarf.

WD 0232+035 is the well-studied post-common envelope binary Feige 24 with an orbital period of 4.23 days (Thorstensen et al. 1978), and the white dwarf is very likely accreting from the M-dwarf companion.

WD 0252−055 (IP Eri) is K0IV+DA binary (Burleigh et al. 1997; Merle et al. 2014). The orbital period of 1071 ± 1.8 day and the low mass, $\simeq 0.4\,M_\odot$, of the white dwarf unambiguously demonstrate past binary interactions (Siess et al. 2014).

WD 0353+284 (V1092 Tau) is a K2V+DA binary in a hierarchical triple, and is unresolved by *Gaia*, implying a projected separation is $\lesssim 0\farcs2$. The companion to the white dwarf is a Barium star (Jeffries & Smalley 1996), suggesting past interaction.

WD 0354−368 is a G2V+DA binary, resolved in the *HST* imaging (Barstow et al. 2001).

WD 0457−103 (63 Eri) is a G4V+DA binary (Landsman et al. 1993; Vennes et al. 1998), unresolved in *HST* (Barstow et al. 2001). The orbital period of 903 ± 5 days (Merle et al. 2016) and the low mass, $\simeq 0.35\,M_\odot$, of the white dwarf unambiguously demonstrate past binary interactions.

WD 0501+524 is an extremely well-studied flux standard; however, little information is available on its common proper motion companion. Its absolute magnitude, $G \simeq 5.9$, suggests that it is an early K-type star.

WD 0512+326 (14 Aur C) is a F2V+DA (Vennes et al. 1998) binary which is part of the complex multiple system 14 Aur. There is some confusion in the literature regarding the make-up of this system. The most luminous component, 14 Aur A, is a $V = 5$ δ-Scuti A-star, (Fitch & Wisniewski 1979), which is also a single-lined spectroscopic binary with a 3.79 day orbital period. The nature of its companion is now known. 14 Aur C is a $V = 7.9$ F2V star, and its EUV excess revealed the presence of a hot white dwarf companion (Hodgkin et al. 1993). Optical spectroscopy showed that 14 Aur C is also a single-lined spectroscopic binary with a period of 2.99 days (Tokovinin 1997; Vennes et al. 1998). *HST* imaging, however, resolved 14 Aur C into two components, Ca and Cb. Based on the absence of radial velocity variations in the ultraviolet spectra of the white dwarf (Holberg et al. 1999), (Barstow et al. 2001) associate the

white dwarf with Cb, and argue that 14 Aur is, in fact, a quintuple system.

WD 0659+130 is an unresolved K0IV+DA binary (Vennes et al. 1997), the K-star is a Barium star (Kong et al. 2018), indicative of past interactions.

WD 0905−724 (G Car) is a M0.5IIIa+DA binary, unresolved in *HST* imaging (Barstow et al. 2001). The red giant is a Barium star (Lu 1991), indicating past interaction.

WD 1021+266 (HD 90052) is an F0V+DA binary (Vennes et al. 1998), unresolved in the *HST* imaging (Barstow et al. 2001).

WD 1024+326 is a G5V+DA binary (Genova et al. 1995). The binary is unresolved by *Gaia*, i.e., the projected separation is $\lesssim 0''.2$.

WD 1029+537 has a newly identified common proper motion companion, *Gaia* DR2 850146823002877440, the absolute magnitude of $\simeq 7.3$ suggests the companion suggests a late K-dwarf.

WD 1040+492 has a newly identified common proper motion companion, *Gaia* DR2 835516068448830464, the absolute magnitude of $\simeq 4.9$ suggests that it is a G-dwarf.

WD 1109−225 (β Crt) is an A2IV+DA binary (Fleming et al. 1991), unresolved in *HST* imaging (Barstow et al. 2001). The low mass of the white dwarf, $\simeq 0.4\,M_\odot$ (Burleigh et al. 2001), suggests past binary interactions. While there is some dispute on the radial velocity variability of this binary (Duemmler et al. 1997; Smalley et al. 1997), observations obtained so far suggest that it is not a short-period binary. The somewhat elevated ASTROMETRIC_EXCESS_NOISE of 1.6 may be an indication of an astrometric perturbation due to the orbital motion.

WD 1528+487 has a newly identified common proper motion companion, *Gaia* DR2 1402147706492229376, the absolute magnitude of $\simeq 3.6$ suggests that it is a mid F-type dwarf.

WD 1550+130 is a short-period, 3.07 hr, eclipsing post-common envelope binary (Haefner 1989), and the white dwarf is very likely accreting from the M-dwarf companion.

WD 1603+432 has a newly identified common proper motion companion, *Gaia* DR2 1385162244706381312, the absolute magnitude of $\simeq 14$ and the *Gaia* $G_{\rm bp}-G_{\rm rp} = 1.05$ color suggests the companion is a second, cool white dwarf. Indeed, the companion is flagged as a white dwarf candidate with a photometric temperature of $\simeq 5200$ K (Gentile Fusillo et al. 2019).

WD 1620−391 is a common proper motion companion to the G5V star HD 147513, which hosts a Jupiter mass planet with a 528.4 days period (Mayor et al. 2004).

WD 1635+529 (16 Dra) is a B9.5V+DA binary (Burleigh & Barstow 2000). *Gaia* resolves the binary with a projected separation of 11.5 arc Section 16 Dra is a common proper motion companion to 17 Dra, itself being a B9V+A1V binary.

WD 1734+742 (29 Dra, DR Dra) is a K0III+DA binary, with a 903.8 ± 0.4 day orbital period (Fekel et al. 1993). The companion is a chromospherically active, and Merle et al. (2016) argue for some past binary interactions.

WD 1921−566 is a G5V+DA binary (Barstow et al. 1994; Kawka & Vennes 2010), which was resolved in *HST* imaging (Barstow et al. 2001). The close separation suggests a period of $\lesssim 100$ yr.

WD 2011+398 is a short-period, 0.706 day, post-common envelope binary (Thorstensen et al. 1994), and the white dwarf is very likely accreting from the M-dwarf companion. WD 2124+191 (IK Peg) is moderately short-period, 21.27 days, A8V+DA binary (Harper 1928; Vennes et al. 1998). WD 2257 −073 is a K0V+DA binary in a hierarchical triple with a G0V star (Barstow et al. 1994; Holberg et al. 2014), the binary is unresolved in the *HST* imaging.

WD 2350−706 (HD 223816) is a F5IV+DA binary (Barstow et al. 1994), which has been resolved in *HST* imaging.

ORCID iDs

Matthias R. Schreiber ● https://orcid.org/0000-0003-3903-8009

References

Ayres, T. R. 1997, JGR, 102, 1641
Barstow, M. A., Barstow, J. K., Casewell, S. L., Holberg, J. B., & Hubeny, I. 2014, MNRAS, 440, 1607
Barstow, M. A., Bond, H. E., Burleigh, M. R., & Holberg, J. B. 2001, MNRAS, 322, 891
Barstow, M. A., Good, S. A., Holberg, J. B., et al. 2003, MNRAS, 341, 870
Barstow, M. A., Holberg, J. B., Fleming, T. A., et al. 1994, MNRAS, 270, 499
Ben-Jaffel, L., & Ballester, G. E. 2013, A&A, 553, A52
Borgniet, S., Lagrange, A. M., Meunier, N., et al. 2019, A&A, 621, A87
Bourrier, V., Lecavelier des Etangs, A., Ehrenreich, D., et al. 2018, A&A, 620, A147
Brown, J. C., Veras, D., & Gänsicke, B. T. 2017, MNRAS, 468, 1575
Bruhweiler, F. C., & Kondo, Y. 1981, ApJL, 248, L123
Burleigh, M. R., & Barstow, M. A. 2000, A&A, 359, 977
Burleigh, M. R., Barstow, M. A., & Fleming, T. A. 1997, MNRAS, 287, 381
Burleigh, M. R., Barstow, M. A., Schenker, K. J., et al. 2001, MNRAS, 327, 1158
Casewell, S. L., Dobbie, P. D., Napiwotzki, R., et al. 2009, MNRAS, 395, 1795
Cassan, A., Kubas, D., Beaulieu, J. P., et al. 2012, Natur, 481, 167
Catalán, S., Isern, J., García-Berro, E., et al. 2008, A&A, 477, 213
Chauvin, G., Desidera, S., Lagrange, A. M., et al. 2017, A&A, 605, L9
Chayer, P., Vennes, S., Pradhan, A. K., et al. 1995, ApJ, 454, 429
Dickinson, N. J., Barstow, M. A., & Welsh, B. Y. 2013, MNRAS, 428, 1873
Duemmler, R., Pelt, J., Korhonen, H., & Iliev, I. 1997, A&A, 328, L37
Duncan, M. J., & Lissauer, J. J. 1998, Icar, 134, 303
Ehrenreich, D., Bourrier, V., Bonfils, X., et al. 2012, A&A, 547, A18
Ehrenreich, D., Bourrier, V., Wheatley, P. J., et al. 2015, Natur, 522, 459
Farihi, J. 2016, NewAR, 71, 9
Farihi, J., Hoard, D. W., & Wachter, S. 2006, ApJ, 646, 480
Farihi, J., Hoard, D. W., & Wachter, S. 2010, ApJS, 190, 275
Fekel, F. C., Henry, G. W., Busby, M. R., & Eitter, J. J. 1993, AJ, 106, 2370
Fitch, W. S., & Wisniewski, W. Z. 1979, ApJ, 231, 808
Fleming, T. A., Schmitt, J. H. M. M., Barstow, M. A., & Mittaz, J. P. D. 1991, A&A, 246, L47
Fontaine, G., Brassard, P., & Bergeron, P. 2001, PASP, 113, 409
Gaia Collaboration, Brown, A. G. A., Vallenari, A., et al. 2018, A&A, 616, A1
Genova, R., Bowyer, S., Vennes, S., et al. 1995, AJ, 110, 788
Gentile Fusillo, N. P., Tremblay, P.-E., Gänsicke, B. T., et al. 2019, MNRAS, 482, 4570
Ghezzi, L., Montet, B. T., & Johnson, J. A. 2018, ApJ, 860, 109
Haefner, R. 1989, A&A, 213, L15
Harper, W. E. 1928, PDAO, 4, 171
Hodgkin, S. T., Barstow, M. A., Fleming, T. A., Monier, R., & Pye, J. P. 1993, MNRAS, 263, 229
Holberg, J. B., & Bergeron, P. 2006, AJ, 132, 1221
Holberg, J. B., Burleigh, M. R., & Sion, E. M. 1999, in ASP Conf. Ser. 169, 11th European Workshop on White Dwarfs, ed. S.-E. Solheim & E. G. Meistas (San Francisco, CA: ASP), 531
Holberg, J. B., Casewell, S. L., Bond, H. E., Burleigh, M. R., & Barstow, M. A. 2014, MNRAS, 444, 2022
Holberg, J. B., Oswalt, T. D., Sion, E. M., Barstow, M. A., & Burleigh, M. R. 2013, MNRAS, 435, 2077
Jeffries, R. D., & Smalley, B. 1996, A&A, 315, L19
Jura, M. 2003, ApJL, 584, L91

Jura, M., & Young, E. D. 2014, AREPS, 42, 45

Kalirai, J. S., Hansen, B. M. S., Kelson, D. D., et al. 2008, ApJ, 676, 594

Kawka, A., & Vennes, S. 2010, in ASP Conf. Ser. 435, Binaries—Key to Comprehension of the Universe, ed. A. Prša & M. Zejda (San Francisco, CA: ASP), 189

Koester, D. 2010, MmSAI, 81, 921

Koester, D., Gänsicke, B. T., & Farihi, J. 2014, A&A, 566, A34

Kong, X. M., Zhao, G., Zhao, J. K., et al. 2018, MNRAS, 476, 724

Landsman, W., Simon, T., & Bergeron, P. 1993, PASP, 105, 841

Lu, P. K. 1991, AJ, 101, 2229

Marois, C., Macintosh, B., Barman, T., et al. 2008, Sci, 322, 1348

Mayor, M., & Queloz, D. 1995, Natur, 378, 355

Mayor, M., Udry, S., Naef, D., et al. 2004, A&A, 415, 391

Merle, T., Jorissen, A., Masseron, T., et al. 2014, A&A, 567, A30

Merle, T., Jorissen, A., Van Eck, S., Masseron, T., & Van Winckel, H. 2016, A&A, 586, A151

Murray-Clay, R. A., Chiang, E. I., & Murray, N. 2009, ApJ, 693, 23

Owen, J. E. 2019, AREPS, 47, 67

Owen, J. E., & Alvarez, M. A. 2016, ApJ, 816, 34

Owen, J. E., & Wu, Y. 2017, ApJ, 847, 29

Parker, E. N. 1964, ApJ, 139, 72

Paxton, B., Bildsten, L., Dotter, A., et al. 2011, ApJS, 192, 3

Pizzolato, N., Maggio, A., & Sciortino, S. 2000, A&A, 361, 614

Pyrzas, S., Gänsicke, B. T., Brady, S., et al. 2012, MNRAS, 419, 817

Sanz-Forcada, J., Micela, G., Ribas, I., et al. 2011, A&A, 532, A6

Schatzman, E. 1948, Natur, 161, 61

Shapiro, S. L., & Lightman, A. P. 1976, ApJ, 204, 555

Shvartzvald, Y., Maoz, D., Udalski, A., et al. 2016, MNRAS, 457, 4089

Siess, L., Davis, P. J., & Jorissen, A. 2014, A&A, 565, A57

Smalley, B., Kellett, B. J., Wonnacott, D., & Stickland, D. J. 1997, MNRAS, 284, 457

Suzuki, D., Bennett, D. P., Sumi, T., et al. 2016, ApJ, 833, 145

Thorstensen, J. R., Charles, P. A., Bowyer, S., & Margon, B. 1978, ApJ, 223, 260

Thorstensen, J. R., Vennes, S., & Shambrook, A. 1994, AJ, 108, 1924

Tian, F., Toon, O. B., Pavlov, A. A., & De Sterck, H. 2005, ApJ, 621, 1049

Tokovinin, A. A. 1997, A&AS, 121, 71

Tripathi, A., Kratter, K. M., Murray-Clay, R. A., & Krumholz, M. R. 2015, ApJ, 808, 173

Tu, L., Johnstone, C. P., Güdel, M., & Lammer, H. 2015, A&A, 577, L3

Vennes, S., Christian, D. J., Mathioudakis, M., & Doyle, J. G. 1997, A&A, 318, L9

Vennes, S., Christian, D. J., & Thorstensen, J. R. 1998, ApJ, 502, 763

Veras, D. 2016, MNRAS, 463, 2958

Vidal-Madjar, A., Désert, J.-M., Lecavelier des Etangs, A., et al. 2004, ApJL, 604, L69

Vidal-Madjar, A., Lecavelier des Etangs, A., Désert, J.-M., et al. 2003, Natur, 422, 143

Wang, Y.-M. 1981, A&A, 102, 36

Weidemann, V. 2000, A&A, 363, 647

Williams, K. A., Bolte, M., & Koester, D. 2009, ApJ, 693, 355

Xu, S., Jura, M., Koester, D., Klein, B., & Zuckerman, B. 2014, ApJ, 783, 79

Yelle, R., Lammer, H., & Ip, W.-H. 2008, SSRv, 139, 437

Zuckerman, B., Koester, D., Reid, I. N., & Hünsch, M. 2003, ApJ, 596, 477